

Optical beam shaping and diffraction free waves: a variational approach

John A. Gemmer^{a,*}, Shankar C. Venkataramani^{b,c}, Charles G. Durfee^d,
Jerome V. Moloney^{b,c,e}

^a*Division of Applied Mathematics, Brown University, Providence, RI 02912, U.S.A.*

^b*Arizona Center for Mathematical Sciences, Department of Mathematics, University of Arizona, Tucson, AZ 85721, U.S.A.*

^c*Department of Mathematics, University of Arizona, Tucson, AZ 85721, U.S.A.*

^d*Department of Physics, Colorado School of Mines, Golden, CO 80401, U.S.A.*

^e*College of Optical Sciences, University of Arizona, Tucson, AZ 85721, U.S.A.*

Abstract

We investigate the problem of shaping radially symmetric annular beams into desired intensity patterns along the optical axis. Within the Fresnel approximation, we show that this problem can be expressed in a variational form equivalent to the one arising in phase retrieval. Using the uncertainty principle we prove various rigorous lower bounds on the functional; these lower bounds estimate the L^2 error for the beam shaping problem in terms of the design parameters. We also use the method of stationary phase to construct a natural *ansatz* for a minimizer in the short wavelength limit. We illustrate the implications of our results by applying the method of stationary phase coupled with the Gerchberg-Saxton algorithm to beam shaping problems arising in the remote delivery of beams and pulses.

Keywords: Beam shaping; Localized waves; Phase retrieval; Paraxial wave equation; Fresnel approximation

1. Introduction

1.1. Physical description and motivation of the problem

In many applications it is desirable to shape a beam or pulse of light so that it has specific properties along the optical axis. In particular, for applications in microscopic imaging [1], optical tweezers [2], laser micro-machining [3], dressing of optical filaments [4], filament formation [5] and long-range laser ablation [6, 7], to name a few, it is important to have a well controlled beam with a nearly uniform intensity along the optical axis. However, due to their wave nature localized packets of light will broaden spatially through diffraction. For

*Principal corresponding author

Email address: john_gemmer@brown.edu (John A. Gemmer)

example, Gaussian beams of width W_0 and wavenumber k double in spatial extent over the Rayleigh range $z_R \sim W_0^2 k/2$ [8].

In a linear, isotropic medium the electric field of a beam of light polarized in the $\hat{\mathbf{e}}$ direction can be modeled by a wave packet of the form $\mathbf{E}(\mathbf{x}_\perp, z) = E(x, y, z) \exp(ikz - i\omega_0 t) \hat{\mathbf{e}}$, where $z \in \mathbb{R}^+$ denotes the spatial coordinate along the optical axis, $x, y \in \mathbb{R}$ are the Cartesian coordinates transverse to the optical axis, $t \in \mathbb{R}^+$ is time and ω_0 the carrier angular frequency of the wave. Within the slowly varying *ansatz* on E , the propagation of a beam with initial data $E(x, y, 0) = E_0 f(x, y)$ at the $z = 0$ plane is described by the paraxial wave equation:

$$\begin{cases} \frac{\partial E}{\partial z} = \frac{i}{2k} \Delta_\perp E, \\ E(x, y, 0) = E_0 f(x, y) \end{cases} \quad (1.1)$$

where Δ_\perp is the transverse Laplacian defined by $\Delta_\perp = \partial_x^2 + \partial_y^2$ [9]. Exact solutions to Equation (1.1) can be expressed in terms of an integral transform of the initial profile $f(x, y)$; see Appendix A. This integral transform is in fact equal to the Fresnel diffraction integral [10].

Constructing solutions to (1.1) in free space that resist diffraction over length scales much larger than the Rayleigh range has attracted considerable interest within the optics community. Diffraction free beams are solutions to Equation (1.1) satisfying the condition that for all $z \in \mathbb{R}^+$, $|E(x, y, 0)| = |E(x, y, z)|$. If we make the *ansatz* $E(x, y, z) = A(x, y) \exp(ik'z)$ then diffraction free beams can be found by solving the two dimensional Helmholtz equation. Indeed, plane waves, Bessel beams [11, 12], Mathieu beams [13] and parabolic beams [14] are examples of such solutions in various orthogonal coordinate systems.

Note, however, that the diffraction free beams described above are not realizable in practice since they carry infinite energy. One technique for obtaining finite energy approximations of such solutions is apodization at the input plane $z = 0$. That is, if $E(x, y, z)$ solves (1.1) then apodized approximations to $E(x, y, z)$ are found by solving (1.1) with the initial data $E(x, y, 0)f(x, y)$ where $f(x, y)$ is a function of finite extent. In [15] so called ‘‘Bessel-Gauss’’ beams were created by apodizing Bessel beams with a Gaussian function and a general framework for constructing Gaussian apodized solutions to (1.1) was developed in [16] and [17].

Bessel-Gauss beams have received considerable interest because they can be produced experimentally, for example by a diffraction grating with concentric grooves [18]. Alternatively, a Gaussian beam passing through an axicon lens produces a ring beam with a truncated Gaussian cross-section that results from the division of the beam around the axicon tip [19]. The effect of these optical elements is to create a linear superposition of Gaussian beamlets whose individual wave vectors $k = k_\perp \sin(\theta)$ lie on a cone of aperture angle θ . The mutual interference of these beamlets generates the Bessel pattern and due to influx of energy supplied by the oscillatory wings of the Bessel function to the central core, these waves are robust to nonlinear losses and physical barriers [20]. However, for a truncation of width W_A the Bessel-Gauss beam only accurately approximates the ideal Bessel beam in a ‘‘Bessel-zone’’ of width $z_{BZ} \sim W_A / \tan(\theta)$ near

the tip of the axicon [21] and then transitions to a ring-beam in the far-field [15, 22].

It was also shown by Bagini et. al. [22] that Bessel-Gauss beams can be created remotely by focusing ring beams. Specifically, in cylindrical coordinates (r, θ, z) Bessel-Gauss beams can be generated remotely by solving Equation (1.1) with the initial data

$$E(r, 0) = E_0 \exp\left(-\frac{r^2 + a^2}{W_0^2}\right) J_0\left(i\frac{2ar}{z_d} + \beta r\right), \quad (1.2)$$

where E_0 is the peak value of the electric field, a is the radius of the ring beam, W_0 is the characteristic width of the ring, z_d is the focal distance, J_0 is the zero order Bessel function of the first kind and β is a parameter related to the focusing of the beam [22]. Note that for this initial data the argument of the Bessel function is complex valued and in particular if $\beta = 0$ – no focusing – it reduces to a modified Bessel function of the first kind. In Figure 1 we provide a contour plot of the $r - z$ intensity profile for such a “generalized” Bessel-Gauss beams and select four radial cross sections to highlight the transition from a ring-beam into a Bessel-Gauss beam and back to a ring beam. As can be seen from Figure 1, the intensity profile along the optical axis ($r = 0$) is not uniform in z within the Bessel-zone and is in fact given by a Lorentzian-Gaussian type function [15, 22].

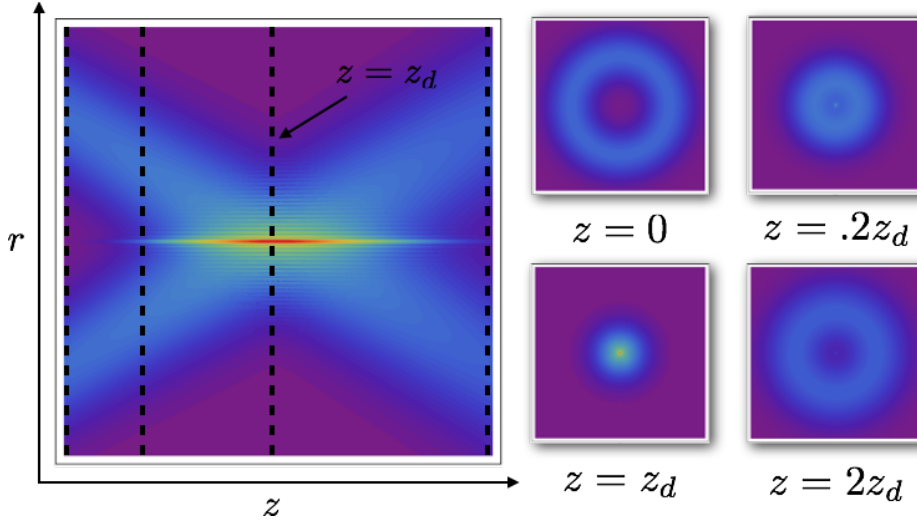


Figure 1: The large image on the left is a contour plot of the square root of the intensity profile for a representative of the generalized Bessel-Gauss beams discovered by Bagini et. al. [22]. The four smaller plots on the right are cross sections of the beam transverse to the optical-axis corresponding to the vertical dashed lines. The figure illustrates the transition of the ring beam into a Bessel-Gauss beam and back into a ring beam in the far field along the optical axis.

The non-uniformity of the on-axis intensity limits the utility of Bessel-beams

in some applications. In this paper we explore the problem of applying additional phase shaping to the ring beam in order to create beams with specific properties along the optical axis. Specifically, we consider the problem of constructing a phase function $\phi(r)$ at the input plane $z = 0$ that focuses a ring beam intensity profile $E_0 f(r)$ of radius r_0 and width W_0 into a target intensity profile $E_T F_T(z)$ of width W_T along the optical axis centered at a target distance z_d . In Figure 2(a) we illustrate the geometry and notation for the problem we are considering. The constants $E_0, E_T > 0$ denote peak values of the electric field and $f(r), F_T$ are smooth, non negative compactly supported functions with a maximum value of 1 supported on the intervals S_f and S_{F_T} defined by

$$S_f = \left\{ r \in \mathbb{R}^+ : |r - r_0| \leq \frac{W_0}{2} \right\} \text{ and } S_{F_T} = \left\{ z \in \mathbb{R}^+ : |z - z_d| \leq \frac{W_T}{2} \right\}, \quad (1.3)$$

respectively. Simultaneous amplitude and phase shaping of the beam will achieve the task and indeed this problem was studied in [23]. However, in practice this is achieved through holographic techniques which are difficult to implement and have low power efficiency [23].

In Figure 2(b) we illustrate one possible method for how phase shaping of ring beams can be achieved. First, a ring beam of radius r_0 and width W_0 is created by passing a collimated beam through an axicon or a concentric diffraction grating. The phase function is then applied, perhaps through a lens with a radially dependent thickness, which focuses the beam into the desired profile.

1.2. Mathematical formulation of the problem

The effect of adding a shaper phase $\phi(r)$ can be realized by solving Equation (1.1) with the initial data $E(r, 0) = E_0 f(r) \exp(i\phi(r))$. The exact solutions to Equation (1.1) can be expressed in terms of a Hankel transform and the field along the optical axis is given by the following relationship:

$$E(0, z) = -\frac{ik}{z} \int_0^\infty E_0 f(\rho) \exp(i\phi(\rho)) \exp\left(\frac{ik\rho^2}{2z}\right) \rho d\rho; \quad (1.4)$$

(see Appendix A). In this paper we consider the problem of optimizing the on-axis profile of the beam in the sense that we are interested in minimizing the L^2 norm:

$$\|E_T F_T(z) - |E(0, z)|\|_{L^2}^2 = \int_{-\infty}^\infty (E_T F_T(z) - |E(0, z)|)^2 dz \quad (1.5)$$

over the space of measurable phase functions ϕ . Note that while the optimal axis is defined by the half-line $z > 0$ we have defined the L^2 norm over the entire real axis. We make this definition as it allows us to use the L^2 isometry between a function and its Fourier transform. Moreover, this definition of the functional penalizes the beam wasting light outside the support of the target intensity distribution.

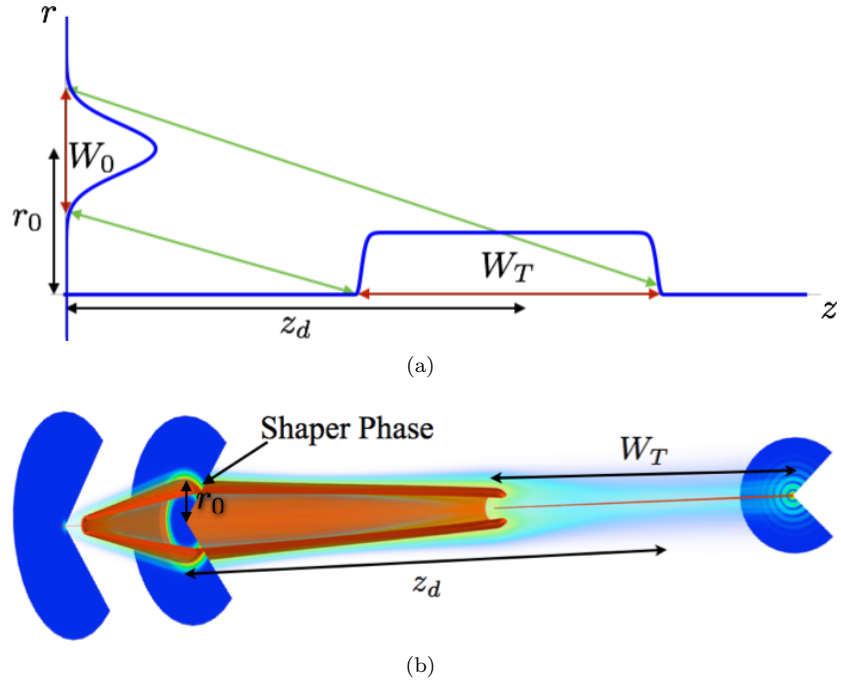


Figure 2: (a) Illustration of the geometry and notation we are using for this problem. (b) The optical setup for the problem we are studying. A beam is first mapped into a cylindrical beam $E_0 f(r)$ of radius r_0 and width W_0 . An optical element is then applied to the cylindrical beam that radially modifies the phase of the cylindrical beam so that the beam is focused a distance z_d into a target intensity profile $E_T F_T(z)$ of width W_T .

Since we are assuming that f is compactly supported away from zero it follows from the change of variables $s = \rho^2$ and $\Omega = k(2z)^{-1}$ that

$$E\left(0, \frac{k}{2\Omega}\right) = -i\Omega\mathcal{F}\left[f(\sqrt{s})e^{i\phi(\sqrt{s})}\right](\Omega), \quad (1.6)$$

where \mathcal{F} denotes the Fourier transform from s -space into Ω -space. The optimal design problem can then abstractly be posed as finding a measurable phase function φ that minimizes the functional $I[\varphi]$ defined by

$$I[\varphi] = \|G(\Omega) - |\mathcal{F}[g(s)\exp(i\varphi(s))]|(\Omega)\|_{L^2}, \quad (1.7)$$

where G and g are positive compactly supported functions. This abstract formulation can be identified with the specific application we are interested in by setting

$$G(\Omega) = \Omega^{-1}E_TE_T\left(\frac{k}{2\Omega}\right), \quad g(s) = E_0f(\sqrt{s}), \quad \varphi(s) = \phi(\sqrt{s}). \quad (1.8)$$

In the two-dimensional setting similar functionals have been studied within the context of shaping beams into desired intensity patterns in the focal plane of a lens [24, 25, 26, 27].

1.3. Connection with phase retrieval

The variational problem we are considering is closely related to the problem of phase retrieval from two intensity measurements, i.e. the problem of determining the complex argument of a function given both knowledge of the modulus of a function and the modulus of its Fourier transform. Phase retrieval arises in applications in various fields ranging from astronomy [28, 29], ultra-short pulses [30], radial beam shaping [31], pulse shaping [32], microscopy [33], to image reconstruction [34]. A detailed review of the history of this problem and a number of numerical techniques that have been developed to solve this problem can be found in [35].

Within the context of phase retrieval, the most common technique for optimizing I is the alternating projection algorithm pioneered by Gerchberg and Saxton [33] and its variants such as the hybrid input-output algorithm discovered by Fienup [36]. In the original Gerchberg-Saxton algorithm the phase is recovered as follows:

1. Choose an initial guess $\phi_0 \in \mathcal{M}$.
2. Define $\Psi_n = \arg(\mathcal{F}[g(s)\exp(i\varphi_{n-1}(s))])$.
3. Define $\phi_n = \arg(\mathcal{F}^{-1}[G(\Omega)\exp(i\Psi_n(\Omega))])$.
4. Loop through items 2 and 3 until $I[\phi_n]$ is sufficiently close to zero.

Through Plancherel's identity it can be shown that the Gerchberg-Saxton algorithm is an error reducing algorithm in the sense that $I[\phi_{n+1}] \leq I[\phi_n]$ [36]. However, this property alone does not guarantee convergence of the algorithm.

While projection algorithms converge on convex sets [37, 38], the projections employed by the Gerchberg-Saxton algorithm are analogous to projections onto the boundary of the unit ball in \mathbb{C} which is clearly not convex. This lack of convexity commonly leads to stagnation of the algorithm away from the global minimum which must be overcome by additional ad hoc means [27, 39, 40]. Indeed, additional techniques such as the hybrid input-output algorithm are commonly implemented along with the Gerchberg-Saxton to force the algorithm out of local minimum [39]. Other techniques for phase retrieval have also been developed including in the two dimensional setting a variational principle for the transport of intensity distributions between two planes orthogonal to the optical axis [41].

In phase shaping, however, the infimum of I may be significantly bounded away from zero and therefore when applied to our problem convergence of the Gerchberg-Saxton algorithm cannot be assessed. Indeed, without any further *a priori* information about the minimum value of I stagnation of the algorithm is the only indication of possible convergence. Moreover, if the Gerchberg-Saxton stagnates at a large value of I it may indeed be at the global minimum for the problem.

1.4. Organization of paper and summary of main results

The paper is organized as follows. In section 2 we use elementary Fourier analysis to deduce some basic results concerning the functional I and translate these results in terms of the practical parameters for the phase shaping problem we are interested in. Using Plancherel's identity we obtain as a necessary condition for accurate beam shaping a normalization for the peak target intensity E_T^2 in terms of the design parameters:

$$E_T^2 = \frac{2\pi k \|f(\sqrt{r})\sqrt{r}\|_{L^2}^2}{\|F_T(z)\|_{L^2}^2} E_0^2. \quad (1.9)$$

We also prove the existence of a minimum for this problem and in doing so obtain the regularity result that the optimal phase is the argument of an analytic function. Finally, in using the uncertainty principle we prove *ansatz free* lower bounds on the minimum value of the functional. Indeed we prove the following necessary condition for accurate beam shaping:

$$\beta = \frac{2kW_TW_0r_0}{4z_d^2 - W_T^2} > \pi. \quad (1.10)$$

Although we discovered this result independently, Romero and Dickey are to the best of our knowledge the first to make the connection between the uncertainty principle and limitations in beam shaping arising from diffraction [42]. Our work goes beyond their treatment in that we prove in a mathematically precise manner the exact range of parameters for which the minimum value is bounded away from zero.

In section 3 we use the stationary phase method to construct a phase $\phi(r)$ such that solutions to Equation (1.1) with the initial data $E(r, 0) = E_0 f(r) \exp(i\phi(r))$ satisfy

$$\lim_{k \rightarrow \infty} |E(0, z)| = E_T F_T(z).$$

The phase is constructed as follows:

1. The following initial value problem is solved:

$$\begin{cases} \frac{dz_c}{d\rho} = 2\pi k \frac{E_0^2 f^2(\rho)}{E_T^2 F_T^2(z_c(\rho))} \rho \\ z_c\left(r_0 - \frac{W_0}{2}\right) = z_d - \frac{W_T}{2} \end{cases}.$$

2. The phase is found by integrating:

$$\phi(\rho) = -k \int_{r_0 - \frac{W_0}{2}}^{\rho} \frac{u}{z_c(u)} du.$$

A similar approach was taken by Friberg in the analysis of a logarithmic axicon lens [43]. While Friberg showed that the logarithmic axicon lens maps the support of f into F_T in the short wavelength limit ($k \rightarrow \infty$), it fails to match the target intensity. Our approach is more general in that for our construction the intensity distribution is exactly matched in the short wavelength limit. We would like to point out, however, that we are not the first to discover the use of the method of stationary phase for beam shaping. Indeed, after we successfully extended Friberg's analysis in [43] to our setting we discovered that Romero and Dickey developed essentially the same algorithm in the two-dimensional setting in [42] and further developed the theory in [44].

In section 4 we explore how the method of stationary phase coupled with the Gerchberg-Saxton algorithm can be applied to practical problems. We consider three specific applications. We first study the problem of creating a near-uniform intensity along the optical axis down range from a source. Specifically, we take the input beam to be a Gaussian ring and the target profile to be a n -th order super-Gaussian. We show that the stationary phase approximation yields a good initial guess that is further improved upon by the Gerchberg-Saxton algorithm. We also highlight the role of the uncertainty principle and show that accurate phase shaping is impossible for sufficiently small values of W_0 or W_T . We also consider in this section the problem of creating beams with oscillatory intensity profiles. We show that as a consequence of the uncertainty principle there is a cutoff in the period of these oscillations below which phase shaping cannot adequately match the target intensity. We illustrate this by applying our algorithm to periodic intensity profiles with small scale oscillations. Finally, we show in this section how the method of stationary phase coupled with linear temporal chirping can be used to form pulses with specified temporal widths at the target distance z_d . Specifically, by taking a

separable spatio-temporal *ansatz* on the initial data we show that spatial phase shaping can be employed to correct for the additional spatial spreading of the beam arising from linear temporal chirping.

We conclude with a summary and discussion of our results.

2. Mathematical results obtained through Fourier Analysis

In this section we use the abstract variational formulation of our problem to obtain quantitative information about our beam shaping problem. Let \mathcal{M} denote the space of Lebesgue measurable functions on \mathbb{R} and $C_0^\infty(\mathbb{R}^+)$ the space of smooth compactly supported functions on \mathbb{R}^+ . Recall from the introduction that we are interested in minimizing the functional $I : \mathcal{M} \mapsto \mathbb{R}$ defined by

$$I[\varphi] = \|G - |\mathcal{F}[g \exp(i\varphi)]|\|_{L^2}, \quad (2.1)$$

with $G, g \in C_0^\infty(\mathbb{R}^+)$ having support bounded away from the origin. In terms of the particular beam shaping problem we are interested in the *shaper phase* is given by $\phi(r) = \varphi(r^2)$, the *input profile* of the electric field is given by $f(r) = E_0^{-1}g(r^2)$ and the *target profile* is given by $F_T(z) = \frac{k}{2z}E_T^{-1}G\left(\frac{k}{2z}\right)$. In particular we will assume that the supports of g and G are given by the intervals $S_g(r_0, W_0)$ and $S_G(z_d, W_t)$ defined by

$$S_g(r_0, W_0) = \left\{ s \in \mathbb{R} : \left(r_0 - \frac{W_0}{2} \right)^2 \leq s \leq \left(r_0 + \frac{W_0}{2} \right)^2 \right\} \quad (2.2)$$

and

$$S_G(z_d, W_T) = \left\{ \Omega \in \mathbb{R} : \frac{k}{2z_d + W_T} \leq \Omega \leq \frac{k}{2z_d - W_T} \right\} \quad (2.3)$$

respectively where $r_0, W_0, z_d, W_T > 0$.

2.1. Consequences of Plancherel's theorem

Recall Plancherel's theorem which states that $\sqrt{2\pi}\|g\|_{L^2} = \|\mathcal{F}[g]\|_{L^2}$. The following Lemma immediately follows from Plancherel's identity and applications of the triangle inequality and reverse triangle inequality.

Lemma 2.1. *Let $I : \mathcal{M} \mapsto \mathbb{R}$ be the functional defined by Equation (2.1) with $g, G \in C_0^\infty(\mathbb{R}^+)$ having supports $S_g(r_0, W_0)$ and $S_G(z_d, W_T)$ defined by equations (2.2) and (2.3) respectively. Then,*

$$\left| \|G\|_{L^2} - \sqrt{2\pi} \|g\|_{L^2} \right| \leq \inf_{\phi \in \mathcal{M}} I[\phi] \leq \|G\|_{L^2} + \sqrt{2\pi} \|g\|_{L^2}.$$

If the lower bound in Lemma 2.1 is zero, i.e. $\|G\|_{L^2} = \sqrt{2\pi}\|g\|_{L^2}$, then in terms of the design parameters we are interested in we have that

$$E_T^2 = \frac{2\pi k \|f(r)\sqrt{r}\|_{L^2}^2}{\|F_T(z)\|_{L^2}^2} E_0^2. \quad (2.4)$$

This provides a natural normalization for E_T in terms of E_0 and the L^2 norms for the specific profiles of the input and target intensity patterns. It is important to note that in our initial formulation of the problem we did not specify any constraints on the target electric field. Throughout the rest of this paper we will assume this normalization and hence that $\|G\|_{L^2} = \sqrt{2\pi}\|g\|_{L^2}$ which will be a critical assumption in the stationary phase analysis as well.

2.2. Equivalent variational problems and the existence of a minimum

We can also use Plancherel's identity to obtain functionals that are defined over a larger admissible set but have the same infimum as I . These functionals are easier to analyze and we use them to prove the existence of a minimizer for our original problem.

For $G, g \in C_0^\infty(\mathbb{R}^+)$, define the functional $\bar{I} : \mathcal{M} \times \mathcal{M} \mapsto \mathbb{R}^+$ by

$$\bar{I}[\varphi, \Psi] = \|G \exp(i\Psi) - \mathcal{F}[g \exp(i\varphi)]\|_{L^2}. \quad (2.5)$$

Letting $\theta(\Omega) = \arg(\mathcal{F}[g \exp(i\varphi)](\Omega))$ it follows for a fixed $\varphi \in \mathcal{M}$ that $I[\varphi, \Psi]$ is minimized by setting $\Psi(\Omega) = \theta(\Omega)$. Therefore, $\inf_{\Psi \in \mathcal{M}} \bar{I}[\varphi, \Psi] = I[\varphi]$ and consequently

$$\inf_{\varphi, \Psi \in \mathcal{M}} \bar{I}[\varphi, \Psi] = \inf_{\varphi \in \mathcal{M}} I[\varphi]. \quad (2.6)$$

Let B_1^∞ denote the unit ball in the L^∞ norm. That is,

$$B_1^\infty = \left\{ \zeta \in L^\infty : \text{ess sup}_{x \in \mathbb{R}} |\zeta(x)| \leq 1 \right\}.$$

Define another functional $I' : B_1^\infty \times B_1^\infty \mapsto \mathbb{R}$ by

$$-I'[\zeta, w] = 2\Re(\langle Gw, \mathcal{F}[g\zeta] \rangle). \quad (2.7)$$

Since we are assuming $\|G\|_{L^2} = \sqrt{2\pi}\|g\|_{L^2}$ it follows that

$$\bar{I}[\varphi, \Psi] = 2\|G\|_{L^2} + I'[\exp(i\varphi), \exp(i\Psi)].$$

Therefore, to study minimizers of \bar{I} it is equivalent to study minimizers of I' . Furthermore, we can use the bilinearity of I' to prove the existence of a minimizer for our functional of interest.

Theorem 2.2 (Existence of minimizer). *Let $I' : B_1^\infty \times B_1^\infty \mapsto \mathbb{R}$ be the functional defined by Equation (2.7) with $g, G \in C_0^\infty(\mathbb{R}^+)$ having supports $S_g(r_0, W_0)$ and $S_G(z_d, W_T)$ defined by equations (2.2) and (2.3) respectively. There exists $\bar{\varphi}, \bar{\Psi} \in \mathcal{M}$ such that for all $\zeta, w \in B_1^\infty$*

$$I'[\exp(i\bar{\varphi}), \exp(i\bar{\Psi})] \leq I'[\zeta, w].$$

Proof. To prove the result we proceed in two steps. First we use the direct method to show that minimizers $(\bar{\zeta}, \bar{w})$ of I' over $B_1^\infty \times B_1^\infty$ exist. Second we show that these minimizers satisfy $|\bar{\zeta}(s)| = 1$, $|\bar{w}(\Omega)| = 1$ a.e. and hence $(\bar{\varphi}, \bar{\Psi}) \in \mathcal{M} \times \mathcal{M}$ defined by $\bar{\varphi} = \arg(\bar{\zeta})$, $\bar{\Psi} = \arg(\bar{w})$ are the desired minimum.

Let (ζ_n, ω_n) be a minimizing sequence for I' over $B_1^\infty \times B_1^\infty$. That is,

$$\lim_{n \rightarrow \infty} I'[\zeta_n, \omega_n] = \inf_{\zeta, \omega \in B_1^\infty} I'[\zeta, \omega].$$

By the Banach-Alaoglu theorem B_1^∞ is weak-* compact and hence $B_1^\infty \times B_1^\infty$ is also compact in the product topology. Therefore, reindexing a subsequence if necessary, we can assume without loss of generality that there exists $(\bar{\zeta}, \bar{\omega}) \in B_1^\infty \times B_1^\infty$ such that $\zeta_n \xrightarrow{*} \bar{\zeta}$ and $\omega_n \xrightarrow{*} \bar{\omega}$ [45].

Let $h_n = \mathcal{F}[g\zeta_n]$ and $h = \mathcal{F}[g\bar{\zeta}]$. From weak-* convergence it follows that for fixed Ω that

$$\lim_{n \rightarrow \infty} h_n(\Omega) = \lim_{n \rightarrow \infty} \int_{-\infty}^{\infty} g(s)\zeta_n(s)e^{i\Omega s} ds = \int_{-\infty}^{\infty} g(s)\bar{\zeta}(s)e^{i\Omega s} ds = h(\Omega).$$

Furthermore, for all Ω it follows from Holder's inequality that

$$|G(\Omega)h_n(\Omega) - G(\Omega)h(\Omega)| \leq 2\|G\|_{L^\infty}\|g\|_{L^1}.$$

Therefore, by Lebesgue's Dominated Convergence Theorem it follows that

$$Gh_n \xrightarrow{L^1} Gh.$$

Finally, from weak-* convergence of w_n and the strong convergence of Gh_n it follows that

$$I'[\bar{\zeta}, \bar{\omega}] = \lim_{n \rightarrow \infty} I'[\zeta_n, \omega_n] = \inf_{\zeta, \omega \in B_1^\infty} I'[\zeta, \omega].$$

That is, $(\bar{\zeta}, \bar{\omega})$ minimizes I' over $B_1^\infty \times B_1^\infty$.

Since $g \in C_0^\infty(\mathbb{R}^+)$ we deduce from the Paley-Wiener Theorem that h is analytic and hence has only isolated zeros [46]. Let $\theta(\Omega) = \arg(h(\Omega))$ and $\psi(\Omega) = \arg(\bar{w}(\Omega))$. Therefore,

$$I'[\bar{\zeta}, \bar{\omega}] = -2 \int_{\mathbb{R}} |h(\Omega)| |w(\Omega)| G(\Omega) \cos(\theta(\Omega) - \Psi(\Omega)) d\Omega$$

is minimized if and only if $|\bar{w}(\Omega)| = 1$ a.e. and there exists an integer valued function $m(\Omega)$ such that $\theta(\Omega) = \Psi(\Omega) + 2m(\Omega)\pi$. From Parseval's equality a similar argument proves that $|\zeta(s)| = 1$ a.e.. \square

Corollary 2.3. *Let $I : \mathcal{M} \mapsto \mathbb{R}^+$ be the functional defined by Equation (2.1) with $g, G \in C_0^\infty(\mathbb{R}^+)$ having supports $S_g(r_0, W_0)$ and $S_G(z_d, W_T)$ defined by equations (2.2) and (2.3) respectively. There exists $\bar{\varphi} \in \mathcal{M}$ such that for all $\varphi \in \mathcal{M}$*

$$I[\bar{\varphi}] < I[\varphi].$$

Proof. Let $\bar{I} : \mathcal{M} \times \mathcal{M}$ be the functional defined by Equation (2.5) and let $(\bar{\varphi}, \bar{\Psi}) \in \mathcal{M} \times \mathcal{M}$ be the global minimizer for \bar{I} . If we let

$$\theta(\Omega) = \arg(\mathcal{F}[g \exp(i\varphi)])(\Omega)$$

then without loss of generality we can assume $\Psi = \theta$ and hence

$$I[\bar{\varphi}] = \bar{I}[\bar{\varphi}, \bar{\Psi}] \leq \inf_{\varphi \in \mathcal{M}} I[\varphi].$$

□

Corollary 2.4. *If $I : \mathcal{M} \mapsto \mathbb{R}^+$ is the functional defined by Equation (2.1) with $g, G \in C_0^\infty(\mathbb{R}^+)$ having supports $S_g(r_0, W_0)$ and $S_G(z_d, W_T)$ defined by equations (2.2) and (2.3) respectively then*

$$\inf_{\varphi \in \mathcal{M}} I[\varphi] > 0.$$

Proof. Let $\bar{\varphi} \in \mathcal{M}$ be the global minimizer of I over \mathcal{M} . Since $g \in C_0^\infty(\mathbb{R}^+)$ the Paley-Weiner theorem implies that $\mathcal{F}[g \exp(i\bar{\varphi})]$ is analytic. Therefore, $\mathcal{F}[g \exp(i\bar{\varphi})]$ cannot be compactly supported on \mathbb{R} and since $G \in C_0^\infty(\mathbb{R}^+)$ is compactly supported on $S_G(z_d, W_T)$ it follows that

$$I^2[\bar{\varphi}] \geq \int_{\mathbb{R} \setminus S_G(z_d, W_T)} |\mathcal{F}[g \exp(i\bar{\varphi})]|^2(\Omega) d\Omega > 0.$$

□

Corollary 2.5 (Regularity). *Let $I : \mathcal{M} \mapsto \mathbb{R}^+$ be the functional defined by Equation (2.1) with $g, G \in C_0^\infty(\mathbb{R}^+)$ having supports $S_g(r_0, W_0)$ and $S_G(z_d, W_T)$ respectively. If $\bar{\varphi} \in \mathcal{M}$ minimizes I then $\exp(i\bar{\varphi}(s))$ is analytic.*

Proof. Since $\bar{\varphi}(s)$ minimizes I over \mathcal{M} it follows from Theorem 2.2 that there exists $\bar{\Psi} \in \mathcal{M}$ such that $(\bar{\varphi}, \bar{\Psi})$ minimizes I' . Consequently, from the same argument used in the proof of Theorem 2.2 and Parseval's theorem it follows that

$$\bar{\varphi}(s) = \arg(\mathcal{F}^{-1}[G \exp(i\bar{\Psi})](s)).$$

Since $G \in C_0^\infty(\mathbb{R}^+)$ it follows from the Paley-Wiener Theorem that $\exp(i\bar{\varphi}(s))$ is analytic. □

It follows from the previous corollary that the minimizers of I are well behaved in the sense that they are smooth except possibly for jump discontinuities of 2π .

2.3. Consequences of the Uncertainty Principle

The uncertainty principle quantifies the impossibility of localizing both a function and its Fourier transform [47]. Therefore, if the length of the support of G and g are both sufficiently small then the minimum value of I will necessarily be significantly bounded away from zero. In particular, while Corollary 2.4 quantifies that the minimum value of I is not zero the uncertainty principle can give us quantitative information about how large the minimum value can be. This is made precise by the following theorem.

Theorem 2.6. Let $I : \mathcal{M} \mapsto \mathbb{R}^+$ be the functional defined by Equation (2.1) with $g, G \in C_0^\infty(\mathbb{R}^+)$ having supports $S_g(r_0, W_0)$ and $S_G(z_d, W_T)$ respectively. If $\|G\|_{L^2} = \sqrt{2\pi}\|g\|_{L^2}$, we have the lower bound

$$\inf_{\varphi \in \mathcal{M}} I[\varphi] \geq \|G\|_{L^2} \left(1 - \frac{1}{\sqrt{\pi}} \sqrt{\frac{2kW_T r_0 W_0}{4z_d^2 - W_T^2}} \right).$$

Proof. By the reverse triangle inequality it follows that

$$\begin{aligned} I[\varphi] &= \|G - \mathcal{F}[g \exp(i\varphi)]\|_{L^2} \\ &\geq \left(\int_{S_G(z_d, W_T)} (G(\Omega) - |\mathcal{F}[g \exp(i\varphi)](\Omega)|)^2 d\Omega \right)^{\frac{1}{2}} \\ &\geq \left| \left(\int_{S_G(z_d, W_T)} G^2(\Omega) d\Omega \right)^{\frac{1}{2}} - \left(\int_{S_G(z_d, W_T)} |\mathcal{F}[g \exp(i\varphi)](\Omega)|^2 d\Omega \right)^{\frac{1}{2}} \right| \\ &= \left| \|G\|_{L^2} - \left(\int_{S_G(z_d, W_T)} |\mathcal{F}[g \exp(i\varphi)](\Omega)|^2 d\Omega \right)^{\frac{1}{2}} \right|. \end{aligned}$$

Furthermore, by direct calculation, an application of the Cauchy-Schwarz inequality and Lemma 2.4 we have that

$$\begin{aligned} \left(\int_{S_G(z_d, W_T)} |\mathcal{F}[g \exp(i\varphi)](\Omega)|^2 d\Omega \right)^{\frac{1}{2}} &\leq \sqrt{\frac{2kW_T}{4z_d^2 - W_T^2}} \|\mathcal{F}[g \exp(i\varphi)]\|_{L^\infty} \\ &\leq \sqrt{\frac{2kW_T}{4z_d^2 - W_T^2}} \|g(s)\|_{L^1} \\ &= \sqrt{\frac{2kW_T}{4z_d^2 - W_T^2}} \int_{S_g(r_0, W_0)} |g(s)| ds \\ &\leq \sqrt{\frac{4kW_T r_0 W_0}{4z_d^2 - W_T^2}} \|g\|_{L^2} \\ &= \sqrt{\frac{4kW_T r_0 W_0}{4z_d^2 - W_T^2}} \frac{1}{\sqrt{2\pi}} \|G\|_{L^2}. \end{aligned}$$

□

Using the same notation as in [42] we define the dimensionless parameter β by

$$\beta = \frac{2kr_0 W_T W_0}{4z_d^2 - W_T^2}.$$

It then follows from Theorem 2.6, that $I[\varphi] \geq \|G\|_{L^2} \left(1 - \sqrt{\frac{\beta}{\pi}}\right)$, for any choice of the phase function φ . In particular, if $\beta < \pi$, there is no way of using phase shaping to match the target profile.

We emphasize that the result is only a lower bound for the functional $I[\varphi]$, and in particular it does not follow that if the parameters k, r_0, W_0, W_T and z_d are such that $\beta > \pi$, then the infimum of I is zero. Also, this result is somewhat crude in that it is independent of the exact forms of G and g . Below is a refinement of Theorem 2.6 that takes into account the L^1 norms of g and G .

Theorem 2.7. *Let $I : \mathcal{M} \mapsto \mathbb{R}^+$ be the functional defined by Equation (2.1) with $g, G \in C_0^\infty(\mathbb{R}^+)$ having supports $S_g(r_0, W_0)$ and $S_G(z_d, W_T)$ defined by equations (2.2) and (2.3) respectively.*

1. *If $\|G\|_{L^2} = \sqrt{2\pi}\|g\|_{L^2}$ then*

$$\inf_{\varphi \in \mathcal{M}} I[\varphi] \geq \sqrt{2\pi}\|g\|_{L^2} \left(1 - \sqrt{\frac{2kW_T}{4z_d^2 - W_T^2} \frac{\|g\|_{L^1}}{\|g\|_{L^2}}}\right).$$

2. *If $\|G\|_{L^2} = \sqrt{2\pi}\|g\|_{L^2}$ then*

$$\inf_{\varphi \in \mathcal{M}} I[\varphi] \geq \|G\|_{L^2} \left(1 - \sqrt{\frac{r_0 W_0}{\pi} \frac{\|G\|_{L^1}}{\|G\|_{L^2}}}\right).$$

Proof. Item 1 follows from the proof of Theorem 2.6 and Plancherel's identity. To prove item 2 we note that from Plancherel's identity and the triangle inequality that

$$\bar{I}[\varphi, \Psi] \geq \sqrt{2\pi} \left| \left(\int_{S_g(r_0, W_0)} |\mathcal{F}^{-1}[G \exp(i\Psi)](s)|^2 ds \right)^{\frac{1}{2}} - \|g\|_{L^2} \right|.$$

Following the same arguments as in the proof of Theorem 2.6 it follows that

$$\left(\int_{S_g(r_0, W_0)} |\mathcal{F}^{-1}[G \exp(i\Psi)](s)|^2 ds \right)^{\frac{1}{2}} \leq \frac{1}{2\pi} \sqrt{2r_0 W_0} \|G\|_{L^1}.$$

The result follows from applying Plancherel's identity to $\|g\|_{L^2}$. \square

Theorems 2.6 and 2.7 are estimates for the global error in the beam shaping problem in terms of the design parameters. The same techniques can be used to obtain local information as well. Specifically, the uncertainty principle implies that if G has sufficiently small scale features within its support then the infimum of I will be bounded away from zero. To make this statement precise we look

at the local error for an interval of width W'_T centered at z'_d on the optical axis. Specifically, for all $W'_T, z'_d \in \mathbb{R}^+$ satisfying

$$2z'_d - W'_T > 2z_d - W_T \text{ and } 2z'_d - W'_T < 2z_d - W_T \quad (2.8)$$

define $I_{z'_d}^{W'_T} : \mathcal{M} \mapsto \mathbb{R}^+$ by

$$I_{z'_d}^{W'_T}[\varphi] = \|G - |\mathcal{F}[g \exp(i\varphi)]|\|_{L^2(S_G(z'_d, W'_T))} \quad (2.9)$$

$$= \left(\int_{S_G(z'_d, W'_T)} (G(\Omega) - |\mathcal{F}[g \exp(i\varphi)](\Omega)|)^2 d\Omega \right)^{\frac{1}{2}}, \quad (2.10)$$

which is a local measure of the L^2 error on the interval $|z - z'_d| < W'_T$ along the optical axis. The following corollary follows from the same arguments used to prove Theorem 2.6.

Corollary 2.8. *Let $I_{z'_d}^{W'_T} : \mathcal{M} \mapsto \mathbb{R}^+$ be the functional defined by Equation (2.9) with $g, G \in C_0^\infty(\mathbb{R}^+)$ having supports $S_g(r_0, W_0)$ and $S_G(z_d, W_T)$ defined by equations (2.2) and (2.3) respectively. Suppose z'_d, W'_T satisfy $2z'_d - W'_T > 2z_d - W_T$ and $2z'_d - W'_T < 2z_d - W_T$. If $\|G\|_{L^2} = \sqrt{2\pi}\|g\|_{L^2}$ and*

$$\frac{2kW'_T W_0 r_0}{4(z'_d)^2 - (W'_T)^2} \frac{\|G\|_{L^2}^2}{\|G(\Omega)\|_{L^2(S_G(z'_d, W'_T))}^2} < \pi,$$

then

$$\inf_{\varphi \in \mathcal{M}} I_{z'_d}^{W'_T}[\varphi] \geq \|G\|_{L^2(S_G(z'_d, W'_T))} - \frac{1}{\sqrt{\pi}} \sqrt{\frac{2kW'_T r_0 z'_d}{4(z'_d)^2 - (W'_T)^2}} \|G\|_{L^2}.$$

Corollary 2.9. *Let $I_{z'_d}^{W'_T} : \mathcal{M} \mapsto \mathbb{R}^+$ be the functional defined by Equation (2.9) with $g, G \in C_0^\infty(\mathbb{R}^+)$ having supports $S_g(r_0, W_0)$ and $S_G(z_d, W_T)$ defined by equations (2.2) and (2.3) respectively. Suppose z'_d, W'_T satisfy $2z'_d - W'_T > 2z_d - W_T$ and $2z'_d - W'_T < 2z_d - W_T$. If $\|G\|_{L^2} = \sqrt{2\pi}\|g\|_{L^2}$ and*

$$\frac{2kW'_T}{4(z'_d)^2 - (W'_T)^2} \|g\|_{L^1}^2 \leq \|G\|_{L^2(S_G(z'_d, W'_T))}^2,$$

then

$$\inf_{\varphi \in \mathcal{M}} I_{z'_d}^{W'_T}[\varphi] \geq \|G\|_{L^2(S_G(z'_d, W'_T))} - \sqrt{\frac{2kW'_T}{4(z'_d)^2 - (W'_T)^2}} \|g\|_{L^1}.$$

Remark 2.10. *The local error $I_{z'_d}^{W'_T}$ also provides a lower bound for the global error I . Indeed, if we let*

$$\mathcal{A} = \{(z'_d, W'_T) \in \mathbb{R}^+ \times \mathbb{R}^+ : 2z'_d - W'_T \geq 2z_d - W_T \text{ and } 2z'_d + W'_T \leq 2z_d + W_T\}$$

then a sharper estimate for the lower bound on the global error can be found by considering:

$$\begin{aligned} \inf_{\varphi \in \mathcal{M}} I[\varphi] &\geq \sup_{(z'_d, W'_T) \in \mathcal{A}} \inf_{\varphi \in \mathcal{M}} I_{z'_d}^{W'_T}[\varphi] \\ &\geq \sup_{(z'_d, W'_T) \in \mathcal{A}} \left(\|G\|_{L^2(S_G(z'_d, W'_T))} - \frac{1}{\sqrt{\pi}} \sqrt{\frac{2kW_T r_0 z'_d}{4(z'_d)^2 - (W'_T)^2}} \|G\|_{L^2} \right). \end{aligned} \quad (2.11)$$

3. Stationary Phase Construction

Recall that the method of stationary phase can be used to obtain asymptotic expansions for integrals of the form

$$F(\lambda) = \int_{-\infty}^{\infty} e^{i\lambda H(x)} h(x) dx,$$

where $\lambda > 0$, x is real, H is a smooth real valued function and h is a smooth but not necessarily analytic complex valued function. If H has one critical point at x_c , i.e. $\frac{dH}{dx}|_{x_c} = 0$, and $\frac{d^2 H}{dx^2}|_{x_c} \neq 0$ then

$$F(\lambda) = \exp \left(i\lambda H(x_c) + i \left(\frac{d^2 H}{dx^2} \Big|_{x_c} \right) \right) \sqrt{\frac{2\pi}{\lambda \frac{d^2 H}{dx^2} \Big|_{x_c}}} h(x_c) + \mathcal{O} \left(\frac{1}{\lambda} \right)$$

as $\lambda \rightarrow \infty$ [48]. In this section we show how the method of stationary phase can be used to approximate the on-axis profile of the electric field in the limit of short wavelengths and we show how this approximation can be used to construct initial guesses for the optimal phase.

3.1. Short wavelength limit

First, we must define precisely what we mean by short wavelengths in terms of the input parameters and the length scales in the parameter. Using the geometry of the problem as in Figure 2(b), we define the dimensionless quantities

$$\varrho = \frac{\rho - r_0}{W_0}, \quad \zeta = \frac{z - z_d}{W_T}. \quad (3.1)$$

Equation (1.4) gives the on-axis electric field:

$$\begin{aligned} E(0, z_d + W_T \zeta) &= -\frac{ikE_0 W_0}{z_d + W_T \zeta} \int_{-\frac{1}{2}}^{\frac{1}{2}} f(r_0 + W_0 \varrho) \\ &\quad \times \exp \left(i \left(\phi + k \frac{(r_0 + W_0 \varrho)^2}{2(z_d + W_T \zeta)} \right) \right) (r_0 + W_0 \varrho) d\varrho, \end{aligned} \quad (3.2)$$

where we used the fact that the input profile $E(r, 0)$ is only supported on $[r_0 - W_0/2, r_0 + W_0/2]$.

Assuming $W_0/r_0 \ll 1$, $W_T/z_d \ll 1$, we expand the phase in powers of W_0/r_0 and W_T/z_d to obtain

$$\phi + k \frac{(r_0 + W_0 \varrho)^2}{2(z_d + W_T \zeta)} = \phi + \frac{kr_0^2}{2z_d} - \frac{kr_0^2 W_T \zeta}{2z_d^2} + \frac{kr_0 W_0 \varrho}{z_d} - \frac{kr_0 W_0 W_T \zeta \varrho}{z_d^2} + \dots$$

Note that the first three terms in the expansion of $\frac{k\rho^2}{2z}$ do not depend on both ϱ and ζ jointly. Consequently, they can be absorbed as phase factors in $E_0(r)$ or $E(0, z)$ as below, and they *do not affect the intensity* of the input $E_0(r)$ or the on-axis profile $E(0, z)$. Dropping the higher order terms in W_0/r_0 and W_T/z_d , we get

$$\begin{aligned} zE(0, z)e^{i\frac{kr_0^2 W_T \zeta}{2z_d^2}} &\approx -ikE_0 W_0 e^{i\frac{kr_0^2}{2z_d}} \int_{-\frac{1}{2}}^{\frac{1}{2}} \left[f(r_0 + W_0 \varrho) e^{i\frac{kr_0 W_0 \varrho}{z_d}} \right] \\ &\times e^{i\left(\phi - \frac{kr_0 W_0 W_T \zeta \varrho}{z_d^2}\right)} (r_0 + W_0 \varrho) d\varrho. \end{aligned}$$

with ϱ . In order to use phase variations for optical beam shaping, it is clear that the optical path differences over the relevant region (ϱ, ζ) should be many times the wavelength, so that the beam can interfere with itself. This allows for the possibility of controlling the intensity of the beam as a function of position. Since the variations in ζ and ϱ are $O(1)$ by construction, the preceding calculation determines the correct notion of the short wavelength limit in our problem, namely

$$2\kappa = \frac{kr_0 W_0 W_T}{z_d^2} \gg 2\pi.$$

We include an additional factor of 2 in defining κ so that for $W_T/z_d \ll 1$, the dimensionless parameter β , whose definition was motivated by Theorem 2.6 *is identical* to the non-dimensional wave number κ arising from the analysis of beam shaping using phase variations. This argument therefore gives an alternative physical interpretation of the parameter β – It is the phase variation within the beam arising from the different optical path lengths for different parts of the beam in our geometry (Fig. 2(b)).

3.2. Stationary phase approximation

We now assume $W_0/r_0 \ll 1$, $W_T/z_d \ll 1$, $\beta \gg \pi$ and formally apply the method of stationary phase to approximate the on-axis electric field. Define dimensionless quantities by

$$\bar{\rho} = \frac{\rho}{r_0}, \quad \bar{z} = \frac{z}{z_d}, \quad \bar{k} = \frac{r_0^2 k}{z_d}, \quad \bar{\phi} = \frac{z_d}{kr_0^2} \phi, \quad (3.3)$$

then by Equation (1.4) it follows that the on-axis profile of solutions to the paraxial wave equation is given by

$$E(0, \bar{z}) = -\frac{\bar{k} E_0}{\bar{z}} \int_0^\infty f(\bar{\rho}) \exp\left(i\bar{k} \left(\bar{\phi} + \frac{\bar{\rho}^2}{2\bar{z}}\right)\right) \bar{\rho} d\bar{\rho}. \quad (3.4)$$

If $\bar{\phi}$ is a given smooth function, then for a fixed value of \bar{z} stationary points of the phase can be found by solving the equation

$$\frac{d\bar{\phi}}{d\bar{\rho}} + \frac{\bar{\rho}}{\bar{z}} = 0 \quad (3.5)$$

for $\bar{\rho}$. If $\bar{\phi}$ is a monotone decreasing function in $\bar{\rho}$ and $\bar{\phi}$ is either strictly convex or concave then there exists one solution to this equation for each value of \bar{z} and we can implicitly define a function $\bar{\rho}_c(\bar{z})$ by

$$\bar{\rho}_c(\bar{z}) = -\bar{z} \left. \frac{d\bar{\phi}}{d\bar{\rho}} \right|_{\bar{\rho}_c(\bar{z})}. \quad (3.6)$$

Therefore, if we let $\Psi(\bar{\rho}, \bar{z}) = \bar{\phi} + \bar{\rho}^2/(2\bar{z})$ then by the method of stationary phase it follows that if

$$\left. \frac{d^2\Psi}{d\bar{\rho}^2} \right|_{\bar{\rho}_c(\bar{z})} \neq 0 \quad (3.7)$$

then

$$\frac{\bar{z}}{E_0} |E(0, \bar{z})| = \sqrt{\frac{2\pi\bar{k}}{\left| \frac{\partial^2\Psi}{\partial\bar{\rho}^2} \right|_{\bar{\rho}_c(\bar{z})}}} f(\bar{\rho}_c(\bar{z})) \bar{\rho}_c(\bar{z}) + \mathcal{O}(1) \quad (3.8)$$

as $\bar{k} \rightarrow \infty$.

Equation (3.8) gives quantitative information about how rays of light coming from the ring-beam are mapped to the optical axis in the short wavelength limit. In particular, in the short wavelength limit the function $\bar{\rho}_c(\bar{z})$ can be thought of as a mapping between points on the optical-axis and the input plane. However, we are interested in the inverse relationship. Since $\bar{\phi}$ is either strictly convex or concave it follows by differentiating Equation (3.5) with respect to $\bar{\rho}$ that Equation (3.7) is equivalent to the condition that $\bar{\rho}_c(\bar{z})$ is either monotone increasing or decreasing. Therefore, it follows from the inverse function theorem that $\bar{\rho}_c(\bar{z})$ is invertible with inverse $\bar{z}_c(\bar{\rho})$ and by Equation (3.5) we have that

$$\frac{d\bar{\phi}}{d\bar{\rho}} = -\frac{\bar{\rho}}{\bar{z}_c(\bar{\rho})}. \quad (3.9)$$

Consequently,

$$\frac{d^2\Psi}{d\bar{\rho}^2} = \frac{\bar{\rho}}{\bar{z}_c^2(\bar{\rho})} \frac{d\bar{z}_c}{d\bar{\rho}}. \quad (3.10)$$

Therefore, in terms of $\bar{z}_c(\bar{\rho})$ and Equation (3.8) the on-axis electric field can be approximated by

$$|E(0, \bar{z})| \approx E_0 \sqrt{2\pi\bar{k}} f(\bar{\rho}_c(\bar{z})) \bar{\rho}_c^{\frac{1}{2}}(\bar{z}) \left(\left. \frac{d\bar{z}_c}{d\bar{\rho}} \right|_{\bar{\rho}_c(\bar{z})} \right)^{-\frac{1}{2}}. \quad (3.11)$$

3.3. Algorithm for stationary phase approximation

Equation (3.11) can be used to construct an accurate approximation to an optimal $\bar{\phi}$. Formally, if we set $|E(0, z)| = E_T F_T(z)$ then the following initial value problem must be satisfied:

$$\begin{cases} \frac{d\bar{z}_c}{d\bar{\rho}} = 2\pi\bar{k} \frac{E_0^2 f^2(\bar{\rho})}{E_T^2 F_T^2(\bar{z}_c)} \bar{\rho} \\ \bar{z}_c \left(1 - \frac{W_0}{2r_0}\right) = 1 - \frac{W_T}{2z_d} \end{cases} \quad (3.12)$$

The phase corresponding to \bar{z}_c can then be found by integration:

$$\bar{\phi}(\bar{\rho}) = - \int_{1-\frac{W_0}{2r_0}}^{\bar{\rho}} \frac{u}{\bar{z}_c(u)} du. \quad (3.13)$$

equations (3.12) and (3.13) are a simple system of differential equations whose solution we will use as an approximation to the near optimal phase.

Solutions to (3.12) must also satisfy the additional physical constraint that $\bar{z}_c \left(1 + \frac{W_0}{2r_0}\right) = 1 + \frac{W_T}{2z_d}$, that is, the stationary phase approximation maps the support of f to the support of F_T . The following lemma shows that this condition is met if the normalization (2.4) is satisfied and again highlights the important role this normalization takes.

Lemma 3.1. *If \bar{z}_c is a solution to the initial value problem (3.12) and E_T and E_0 satisfy Equation (2.4) then $\bar{z}_c \left(1 + \frac{W_0}{2r_0}\right) = 1 + \frac{W_T}{2z_d}$.*

Proof. Suppose \bar{z}_c is a solution to the initial value problem (3.12) and $\bar{z}_c \left(1 + \frac{W_0}{2r_0}\right) = z^*$. From the normalization (2.4) and the fact that z_c solves (3.12) it follows that

$$\begin{aligned} \int_{1-\frac{W_T}{2z_d}}^{\bar{z}_c(\bar{\rho})} F_T^2(\bar{z}) d\bar{z} &= 2\pi\bar{k} \frac{E_0^2}{E_T^2} \int_{1-\frac{W_0}{2r_0}}^{\bar{\rho}} f^2(u) u du \\ \Rightarrow \frac{\int_{1-\frac{W_T}{2z_d}}^{\bar{z}_c(\bar{\rho})} F_T^2(z) dz}{\|F_T(z)\|_{L^2}^2} &= \frac{\int_{1-\frac{W_0}{2r_0}}^{\bar{\rho}} f^2(u) u du}{\|f(r)\sqrt{r}\|_{L^2}^2}. \end{aligned}$$

Now, if $z^* < 1 + \frac{W_0}{2r_0}$ then

$$1 > \frac{\int_{1-\frac{W_T}{2z_d}}^{\bar{z}_c(\bar{\rho})} F_T^2(z) dz}{\|F_T(z)\|_{L^2}^2} = \frac{\int_{1-\frac{W_0}{2r_0}}^{1+\frac{W_0}{2r_0}} f^2(u) u du}{\|f(r)\sqrt{r}\|_{L^2}^2} = 1.$$

If $z^* > 1 + \frac{W_0}{2r_0}$ then since $\bar{z}_c(\bar{\rho})$ is a continuous monotone increasing function of $\bar{\rho}$ there exists $r^* < 1 + \frac{W_0}{2r_0}$ such that $z_c(r^*) = 1 + \frac{W_T}{2z_d}$. Consequently,

$$1 = \frac{\int_{1-\frac{W_T}{2z_d}}^{\bar{z}_c(r^*)} F_T^2(z) dz}{\|F_T(z)\|_{L^2}^2} < \frac{\int_{1-\frac{W_0}{2r_0}}^{1+\frac{W_0}{2r_0}} f^2(u) u du}{\|f(r)\sqrt{r}\|_{L^2}^2} = 1.$$

Therefore it follows that $z^* = 1 + \frac{W_T}{2z_d}$. \square

3.4. Off-axis electric field

The full electric field near the Bessel-zone $E(r, z)$ can also be approximated in the focal region $|z - z_d| \lesssim W_T/2$ using the method of stationary phase. In the dimensionless coordinates we obtain through the method of stationary phase that:

$$|E(r, \bar{z})| \approx E_T F_T(\bar{z}) J_0 \left(\frac{\bar{k}r}{2\bar{z}r_0} \bar{\rho}_c(\bar{z}) \right). \quad (3.14)$$

That is, the beam essentially forms a Bessel-beam in the focal region. However, the function J_0 is also a rapidly oscillating function and the above approximation is only valid for radii satisfying $r \sim 2\bar{z}r_0/(\bar{k}\bar{\rho}_c(\bar{z}))$. This expression is not applicable outside the focal region, and of course does not capture the transition of the ring beam into a Bessel-Gauss beam and back into a ring beam.

4. Applications

4.1. Remote Delivery of Bessel Beams

In this subsection we use the method of stationary phase coupled with the Gerchberg-Saxton algorithm to obtain approximations to the optimal phase when the input profile $f(r)$ is Gaussian and the target profile $F_T(z)$ is super-Gaussian. Specifically, for n a positive integer and $W'_0, W'_T > 0$ we assume that

$$f(r) = \exp \left(-\frac{(r - r_0)^2}{W_0'^2} \right) \text{ and } F_T(z) = \exp \left(-\frac{(z - z_d)^{2n}}{W_T'^{2n}} \right). \quad (4.1)$$

Since we are using input and target functions that decay exponentially fast we can use Laplace's method [48] to obtain accurate estimates for the normalization. Directly applying Laplace's method it follows that

$$\|f(r)\sqrt{r}\|_{L^2}^2 = W_0' r_0 \sqrt{\frac{\pi}{2}} + \mathcal{O} \left(\frac{W_0'^2}{r_0^2} \right) \quad (4.2)$$

and explicitly calculating we have that

$$\|F_T(z)\|_{L^2}^2 = W_T' \frac{2}{2^{\frac{1}{2n}}} \Gamma \left(1 + \frac{1}{2n} \right). \quad (4.3)$$

Therefore, by Equation (2.4) it follows that

$$\frac{E_T^2}{E_0^2} \approx \sqrt{2} \pi^{\frac{3}{2}} C(n) \frac{k r_0 W_0'}{W_T'}, \quad (4.4)$$

where $C(n) = 2^{\frac{1}{2n}-1} \left(\Gamma \left(1 + \frac{1}{2n} \right) \right)^{-1}$ is bounded between $\frac{1}{2} \sqrt{\frac{\pi}{2}}$ and $\sqrt{\frac{\pi}{2}}$. Equation (4.4) gives the ratio of the peak intensity of the on-axis profile of the beam to the peak intensity of the input beam.

The input and target functions defined above are not smooth bump functions and strictly speaking the theory and numerical algorithm we developed in the previous two sections does not apply. However, the functions given by Equation (4.1) are Schwartz class and they can be very accurately approximated by non-smooth functions with compact support which in turn can be approximated by smooth functions with compact support [49]. In particular, we truncate these functions by forcing them to be zero for values in which the function is less than $e^{-9} \approx 10^{-4}$. This gives us the following estimates for the width of the supports

$$W_0 = 6W'_0 \text{ and } W_T = 2 \cdot 3^{\frac{1}{n}} W'_T. \quad (4.5)$$

With the above normalization, equations (3.12) and (3.13) can be numerically solved to construct a guess for an optimal phase function ϕ . Using ϕ to initialize the Gerchberg-Saxton algorithm, further corrections to the stationary phase construction can be obtained. To illustrate the potential applicability of our techniques to remote laser ablation, we applied the algorithm outlined in the previous section with 100 iterations of the Gerchberg-Saxton algorithm for various input and target widths with the following parameters fixed

$$z_d = 1000m, \quad r_0 = .3m, \quad k = 9.5 \times 10^6 m^{-1}, \quad n = 4. \quad (4.6)$$

The exact profile along the optical axis is then obtained by applying the fast Fourier transform (FFT) to Equation (1.6). In Figure 3(a) we plot the normalized value of I for both the stationary phase analysis and the Gerchberg-Saxton algorithm for $W'_0 = .07m$ and W'_T ranging from $1m$ to $100m$. For this range of parameters, β varies from $\beta = .4$ to $\beta = 40$. The inset plot in Figure 3(a) illustrates a subset of the profiles obtained for $W'_T = 10m, 50m, 100m$. In Figure 3(b) we plot the normalized value of I for both the stationary phase analysis and the stationary phase analysis coupled with the Gerchberg-Saxton algorithm for W'_0 ranging from $.001m$ to $.1m$ and $W'_T = 20m$. For this range of parameters, β varies from $\beta = .1$ to $\beta = 10$. The inset plot in Figure 3(b) illustrates the intensity profile obtained for $W'_0 = .05m$.

Figures 3(a) and 3(b) also illustrate the important role that β not only plays in terms of the lower bound presented in Theorem 2.6 but also the accuracy of the stationary phase approximation. For $W'_T < 8m$ ($\beta = 3$), the lower bound in Theorem 2.6 is relevant and as is guaranteed by Theorem 2.6 neither the stationary phase approximation nor the Gerchberg-Saxton algorithm, or indeed any other algorithm can yield accurate shaping of the beam. For W'_T ranging from $10m$ to $60m$ ($\beta = 4$ to $\beta = 24$) Theorem 2.6 no longer applies and the stationary phase analysis yields a guess that is further improved upon by the Gerchberg-Saxton algorithm. For $W'_T > 60m$ ($\beta = 24$), the stationary phase analysis yields a very accurate guess that is only slightly improved upon by the Gerchberg-Saxton algorithm.

In Figures 4(a) and 4(b) we plot surface and contour plots of the phase function found by coupling the stationary phase approximation with the Gerchberg-Saxton algorithm for the parameters given by Equation (4.6) with $W'_0 = .07m$

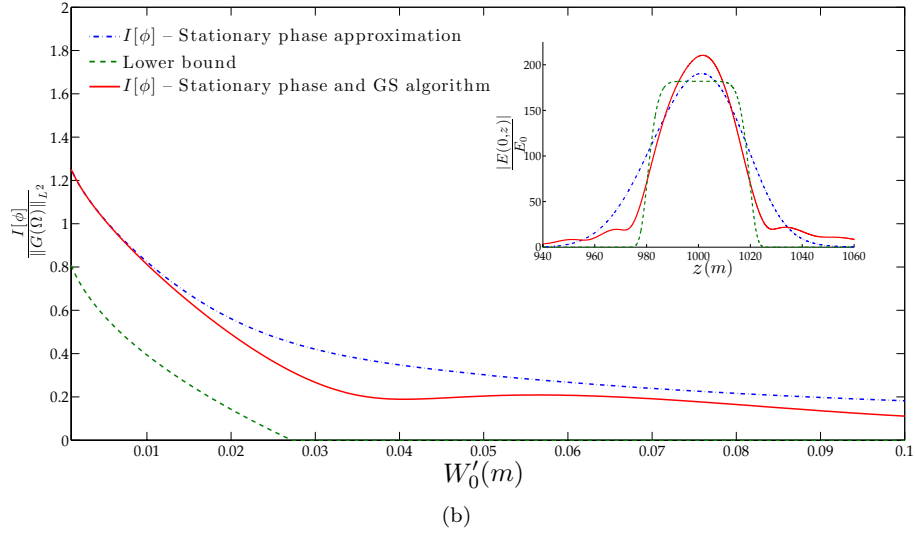
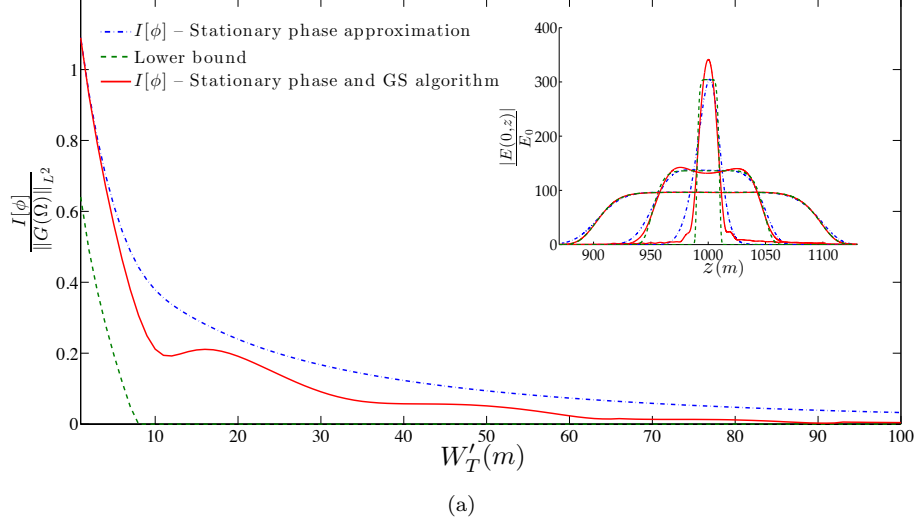


Figure 3: The normalized value of the functional I for phase functions obtained using the stationary phase analysis as an initial guess for the Gerchberg-Saxton algorithm. The fixed parameters in both figures are $r_0 = .3m$, $z_d = 1000m$ and $n = 4$. In the inset plots within each figure the blue dashed-dotted curves are plots of sample on-axis intensities obtained through the stationary phase analysis alone, the solid red curves are the on-axis intensities obtained by coupling the stationary phase algorithm with the Gerchberg-Saxton algorithm and the green dashed curves are the target intensity profile. (a) The value of I for $W'_0 = .07m$ fixed and W'_T ranging from $1m$ to $100m$. The selected intensity profiles in the inset plot have target widths corresponding to $W'_T = 5m$, $50.0m$ and $100m$. (b) The value of I for $W'_T = 20m$ fixed and W'_0 range from $.001m$ to $.1m$.

and W'_T ranging from $5m$ to $100m$. Specifically, we plot

$$\phi_{z_d}(r) = \phi(r) - \frac{kr^2}{2z_d}. \quad (4.7)$$

The term $kr^2/2z_d$ corresponds to a linear shift in the Fourier variable Ω and also has an interpretation in optics as the effect of a lens that focuses a beam at the distance z_d [50]. Interestingly, when $W'_T = 5m$ ($\beta = .4$) the phase ϕ_{z_d} is essentially constant. That is, except for the focusing term $kr^2/2z_d$ additional phase shaping cannot improve upon the effect of a focusing lens. However, for $W'_T = 100m$ ($\beta = 40$) there is a significant difference between the numerically obtained phase and the focusing term. From Figures 4(c) and 4(d) it is again evident that the phase obtained from that Gerchberg-Saxton algorithm converges in the limit of $W_T \rightarrow \infty$ to the one obtained using the stationary phase alone.

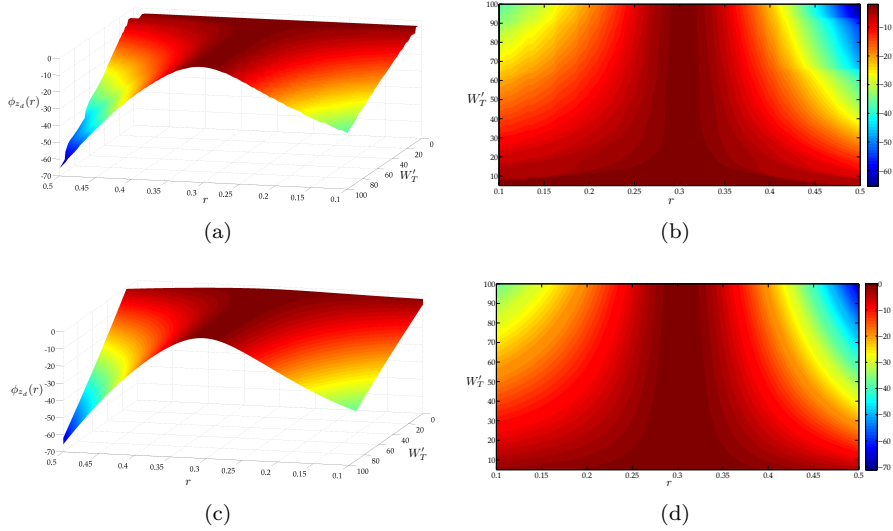


Figure 4: (a) Surface plot of the phase $\phi_{z_d}(r) = \phi(r) - kr^2/2z_d$ obtained by using the method of stationary phase to create an initial guess for 100 iterations of the Gerchberg-Saxton algorithm with $r_0 = .3m$, $W_0 = .07m$, $z_d = 1000m$, $n = 4$ and W'_T ranging from $5m$ to $100m$. (b) Contour plot of $\phi_{z_d}(r)$ for the same range of parameters. (c) Surface plot of the phase $\phi_{z_d}(r) = \phi(r) - kr^2/2z_d$ obtained by using the method of stationary phase. (d) Contour plot of $\phi_{z_d}(r)$ obtained by the method of stationary phase.

In laser ablation while it is important to have a beam with a near uniform on-axis intensity profile, the amount of power delivered by the beam is also of critical importance. In particular, numerical experiments indicate that for critical collapse of a Bessel-Gauss beam to occur the power contained in the central lobe of the beam must be near the critical power of the Townes profile [51]. For a fixed value of z the power delivered by a beam in a circular cross section of

radius R about the optical axis is proportional to the following integral:

$$P_R(z) = \int_0^R |E(r, z)|^2 r dr. \quad (4.8)$$

Using the asymptotic formula (3.14) for the off-axis profile electric field, the power in the central core of the Bessel beam at the target distance $\bar{z} = 1$ can be approximated in the short wavelength limit. If we assume that $\bar{\rho}_c(1) = 1$, then for $\bar{z} = 1$ the electric field is approximately zero at the value $r \approx 4.96r_0/\bar{k}$. Consequently, the power delivered in the central core of the Bessel beam at the distance z_d is approximated by

$$P_C(z_d) \approx E_T^2 F_T^2(z_d) \int_0^{\frac{4.96r_0}{\bar{k}}} J_0^2\left(\frac{\bar{k}r}{2r_0}\right) r dr \approx 3.12 E_T^2 F_T^2(z_d) \frac{z_d^2}{\bar{k}^2 r_0^2}. \quad (4.9)$$

From the normalization (2.4) it follows that in the short wavelength limit we have that:

$$P_C(z_d) \approx 19.6 \frac{F_T^2(z_d)}{\|F_T(z)\|_{L^2}^2} \frac{z_d^2}{\bar{k} r_0^2} P_0,$$

where P_0 is the initial power of the beam. Therefore, from Equation (4.3) it follows that

$$P_C(z_d) \approx 9.8 \times 2^{-\frac{1}{2n}} \Gamma\left(1 + \frac{1}{2n}\right)^{-1} \frac{z_d^2}{\bar{k} r_0^2 W_T'} P_0.$$

This equation illustrates the trade-off between the amount of power delivered within the central lobe and the accuracy of the shaping. In particular, for $\bar{k} \gg 1$ and $W_0' \gg W_0'$ the shaping will be very accurate but the amount of power delivered by the beam in the central core will be much smaller than the initial power of the beam. For the range of parameters used to generate Figure 3(a), for example, this approximation for $P_C(z_d)$ ranges from $.96P_0$ to $.01P_0$.

4.2. Oscillatory patterns

In this subsection we explore the possibility of using beam shaping to create intensity distributions with an oscillatory pattern for length scales that are applicable to micromachining. Again we use a Gaussian input beam:

$$f(r) = \exp\left(-\frac{(r - r_0)^2}{W_0'^2}\right) \quad (4.10)$$

with $r_0 = 50mm$ and $W_0 = 5mm$. For integer values of m we take the target profile to be:

$$F_T(z) = \frac{4}{5} \exp\left(-\frac{(z - z_d)^{16}}{W_T'^{16}}\right) \left(\cos^2\left(\frac{(z - z_d)m}{2\pi W_T'}\right) + \frac{1}{4}\right) \quad (4.11)$$

with $z_d = 1m$, $W_T' = 1mm$ and we take $k = 9.7 \times 10^6 m^{-1}$. As before, we can then apply the method of stationary phase coupled with the Gerchberg-Saxton

algorithm to numerically optimize I . Now, it follows that $\beta = 12.1$ for these parameters and hence Theorem 2.6 is not relevant. However, as the value of m increases the target intensity develops fine scale oscillations of approximate width $w_m = 2W'_T/m$ and therefore by Corollary 2.8 we expect the accuracy of the beam shaping to decrease with increasing m .

As in section 2 define

$$G(\Omega) = \frac{1}{\Omega} E_T F_T \left(\frac{k}{2\Omega} \right) \text{ and } g(s) = E_0 f(\sqrt{r}) \quad (4.12)$$

and for $0 < w_m < W_T$ define the interval $S_G(z_d, w_m)$ by

$$S_G(z_d, w_m) = \left\{ \Omega \in \mathbb{R} : \frac{k}{2z_d + w_m} \leq \Omega \leq \frac{k}{2z_d - w_m} \right\}. \quad (4.13)$$

To capture the influence of the small scale oscillations on the error we define the following local quantity:

$$\delta_m = \frac{\int_{S_G(z_d, w_m)} G^2(\Omega) d\Omega - \frac{2kw_m}{4z_d^2 - w_m^2} \|g(s)\|_{L^1}}{\int_{S_G(z_d, w_m)} G^2(\Omega) d\Omega} \quad (4.14)$$

which is a local measure of the error in matching the target intensity within one period. From Corollary 2.8 it follows that if $\delta_m > 0$ then the small scale oscillations cannot be matched by any phase function.

In Figure 5 we plot the on-axis intensity profiles for the beams obtained by using the stationary phase as an initial guess for the Gerchberg-Saxton algorithm with 100 iterations. We selected the values $m = 1, 5, 10, 15$ to illustrate the influence of m on the accuracy of the shaping. As we can see, with increasing m the method of stationary phase yields a guess that matches the support of the function but fails to capture the small scale oscillations. For these values of m we have that $\delta_1 = -8.6$, $\delta_5 = -.92$, $\delta_{10} = .04$ and $\delta_{15} = .3$ and indeed for $m = 10, 15$, as is to be expected, the Gerchberg-Saxton algorithm cannot match the target intensity. It is interesting to note, however, for large m that although the Gerchberg-Saxton algorithm fails to capture the amplitude of the oscillations it does a decent job recovering the period.

4.3. Remote delivery of Gaussian pulses

In this subsection we show that for a linear medium and under the paraxial approximation the techniques we developed in this paper can be combined with linear temporal chirping to remotely deliver pulses with a desired temporal width at a target distance. The governing equation for such pulses is the temporal paraxial wave equation:

$$\frac{\partial E}{\partial z} = \frac{i}{2k} \Delta_{\perp} E - i \frac{\gamma}{2} \frac{\partial^2 E}{\partial t^2}, \quad (4.15)$$

where γ is the group velocity dispersion for a pulse with wavenumber k [9]. If we assume separable initial data of the form $E(r, 0, t) = H(r)T(t)$ then the

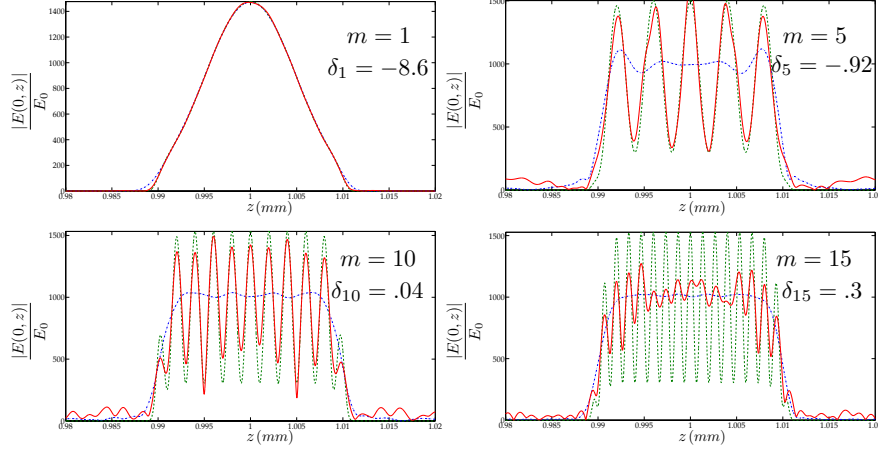


Figure 5: Intensity profiles obtained by the stationary phase method coupled with the Gerchberg-Saxton algorithm for $m = 1, 5, 10, 15$. The blue dashed-dotted curves are the on-axis intensities obtained through the stationary phase analysis alone, the solid red curves are the on-axis intensities obtained by coupling the stationary phase algorithm with the Gerchberg-Saxton algorithm and the green dashed curves are the target intensity profile. The function δ_m quantifies the accuracy of the beam shaping and in particular for $\delta_m > 0$ the amplitude of the oscillations is not matched.

solution to Equation (4.15) can be expressed in terms of the Hankel transform of a convolution:

$$E(r, z, t) = \frac{-ik}{z^{3/2}\sqrt{\pi\gamma}\sqrt{1-i}} \int_0^\infty \int_{-\infty}^\infty H(r) \exp\left(\frac{ik(r^2 + \rho^2)}{2z}\right) J_0\left(\frac{k\rho r}{z}\right) \times T(t') \exp\left(-i\frac{(t-t')^2}{2z\gamma}\right) \rho d\rho dt'. \quad (4.16)$$

Again, we assume that the input spatial profile is given by $H(r) = E_0 f(r) \exp(i\phi(r))$, where $E_0 > 0$, $f \in C_0^\infty(\mathbb{R}^+)$ is supported on the interval $r_0 - W_0/2 < r < r_0 + W_0/2$ and ϕ is a measurable function corresponding to a shaper phase. We assume that the input temporal profile is a linearly chirped Gaussian pulse:

$$T(t) = \exp\left(-\frac{t^2}{\tau_0^2}\right) \exp\left(i\frac{t^2}{\alpha^2}\right) \quad (4.17)$$

where $\tau_0 > 0$ is a measure of the temporal width of the initial pulse and $\alpha > 0$ is a linear chirping parameter. With this initial data, the on-axis intensity is given by

$$|E(0, z, t)| = \frac{k}{z(q(z))^{1/4}} \exp\left(-\frac{t^2}{\tau_0^2 q(z)}\right) \left| \int_0^\infty E_0 f(\rho) \exp(i\phi(\rho)) \exp\left(i\frac{\rho^2}{2z}\right) \rho d\rho \right|, \quad (4.18)$$

with $q(z)$ a quadratic function defined by

$$q(z) = \left(1 - \frac{2z\gamma}{\alpha^2}\right)^2 + \frac{4z^2\gamma^2}{\tau_0^4}. \quad (4.19)$$

The function $q(z)$ quantifies how the temporal width broadens or contracts as it propagates; indeed the characteristic temporal width is $W(z) = \tau_0\sqrt{q(z)}$.

We assume that the target profile along the optical axis is also given by a Gaussian pulse of the form

$$E_T(z, t) = E_T F_T(z) \exp\left(-\frac{t^2}{\tau_T^2}\right), \quad (4.20)$$

where $E_T > 0$, $F_T \in C_0^\infty(\mathbb{R}^+)$ with support $z_d - W_T/2 < z < z_d + W_T/2$ and $\tau_T > 0$. To ensure that $W(z)$ matches the desired temporal width at z_d and the change in $W(z)$ over the support of F_T is as small as possible we must have that

$$W(z_d) = \tau_T \text{ and } \left.\frac{dW}{dz}\right|_{z_d} = 0.$$

Solving these equations yields the conditions:

$$\alpha^2 = \frac{\tau_T^4 + 4z_d^2\gamma^2}{2z_d\gamma} \text{ and } \tau_0^2 = \frac{\tau_T^4 + 4z_d^2\gamma^2}{\tau_T^2}. \quad (4.21)$$

Define $G(\Omega)$ by

$$G(\Omega) = \frac{k \left(q\left(\frac{k}{2\Omega}\right)\right)^{\frac{1}{4}}}{\Omega} F_T\left(\frac{k}{2\Omega}\right) \quad (4.22)$$

and as we did before define $g(s) = E_0 f(\sqrt{s})$, $\varphi(s) = \phi(\sqrt{s})$. The problem of designing the optimal shaper phase with this temporal chirping then corresponds to minimizing the functional $I : \mathcal{M} \mapsto \mathbb{R}^+$ defined by $I[\varphi] = \|G - |\mathcal{F}(g \exp(i\varphi))|\|_{L^2}$ which problem corresponds to the variational problem we considered before except for the additional term

$$k \left(q\left(\frac{k}{2\Omega}\right)\right)^{\frac{1}{4}} \Omega^{-1}$$

accounting for the additional modification to the spatial intensity arising from temporal broadening.

In Figure 6 we plot the on-axis spatial-temporal profile for a Gaussian pulse propagating in air obtained by using the method of stationary phase. For this figure we again assumed that

$$f(r) = \exp\left(-\frac{(r - r_0)^2}{W_0'^2}\right) \text{ and } F_T(z) = \exp\left(-\frac{(z - z_d)^{2n}}{W_T'^{2n}}\right), \quad (4.23)$$

with

$$z_d = 1000m, \quad r_0 = .5m, \quad k = 7.9 \times 10^6 m^{-1}, \quad n = 8$$

$$W'_0 = .1m, \quad W'_T = 20m.$$

Following the experimental results in [52] we took the group velocity dispersion of air for this wavelength of light to be $\gamma = 20(\text{fs})^2 m^{-1}$ and we assumed a target temporal width of $\tau_T = 50\text{fs}$. For these values the initial temporal width is $\tau_0 \approx 800\text{fs}$ and the chirping parameter is $\alpha = 200\text{fs}$.

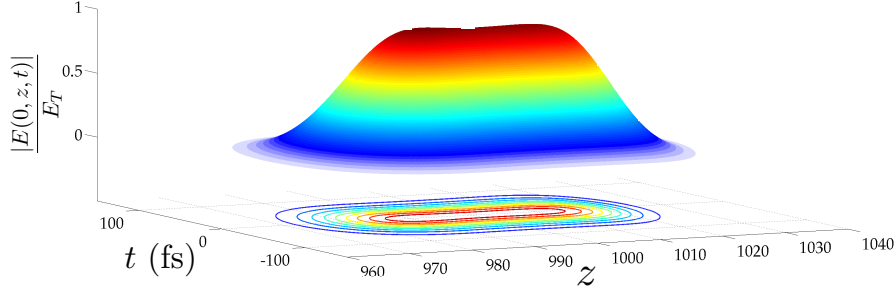


Figure 6: Spatial temporal profile of a Gaussian pulse with near uniform on-axis intensity propagating in the atmosphere. The profile was obtained using the method of stationary phase.

5. Summary and discussion

In this paper we studied the problem of phase shaping an annular beam into a desired intensity profile along the optical axis by analyzing minimizers of the functional $I : \mathcal{M} \mapsto \mathbb{R}$ defined by Equation 2.1. Formally, this functional is equivalent to the ones arising in phase retrieval from two intensity measurements. Typically, due to its speed and ease of implementation, the Gerchberg-Saxton algorithm is used to construct approximate minimizers. While the Gerchberg-Saxton algorithm is an error reducing algorithm there are no known general convergence results for this algorithm. In particular the algorithm typically stagnates away from the global minimum which in phase retrieval can be overcome by additional modifications to the algorithm such as the hybrid input-output method [36] or those in [27]. Moreover, in phase retrieval the infimum of I is zero and convergence of the Gerchberg-Saxton algorithm and its modifications can be assessed by the proximity of I to zero. However, as a consequence of the uncertainty principle the minimum value of I may be significantly bounded away from zero. Consequently it is not clear if modifications to the Gerchberg-Saxton algorithm are applicable to beam shaping problems nor is it clear what a sufficient convergence criterion of such an algorithm would be.

The central result of our work is the identification of the dimensionless quantity

$$\beta = \frac{2kr_0 W_T W_0}{4z_d^2 - W_T^2}$$

and the associated lower bounds on the functional I . We identified three scaling regimes for β for which different quantitative and qualitative behaviors of the optimal profile occur. These regimes are as follows.

1. For $\beta \ll \pi$ the uncertainty principle guarantees that the optimal profile will differ significantly from the target profile. This result has the consequence that neither the Gerchberg-Saxton algorithm nor any other numerical algorithm will yield accurate shaping of the beam.
2. For $\beta \gg \pi$ the method of stationary phase yields an approximation to the problem that is very close to the optimal profile. This asymptotic regime can be considered within the geometrical optics setting in the sense that the light rays originating from the input plane can be accurately mapped to the target intensity profile through the method of stationary phase. Indeed, for the problem of creating a beam with a nearly uniform on-axis intensity, the Gerchberg-Saxton algorithm coupled with the method of stationary phase yields nearly optimal profiles. In particular, the method of stationary phase can be used as a robust method for overcoming the stagnation issues of the Gerchberg-Saxton algorithm commented on in [53].
3. For the intermediate regime where $\beta \sim \pi$ the phase produced by the method of stationary phase is significantly improved upon by the Gerchberg-Saxton algorithm. However, in this asymptotic regime the uncertainty principle no longer applies. Moreover, the value of I for ϕ obtained through the method of stationary phase is not close to zero. Consequently, within this regime there is no clear convergence of the algorithm. Following the reasoning in Remark 2.10 we could obtain more accurate lower bounds on the functional that account for the specific forms of the input and target intensity profile instead of simply the widths of their supports. However, in the regime $\beta \sim \pi$ a universal scaling law for the error in terms of the wavelength is not possible.

The functional we considered was derived under the paraxial assumption and hence is applicable for linear beams with the same range of wavelengths and geometrical length scales as in the Fresnel approximation. Indeed, for the range parameters we considered in the applications, the Fresnel number ranges from 150 to 4000. Consequently, for these parameters the integral transform given by Equation (1.4) very accurately approximates the propagation of the on-axis electric field for linear beams. Therefore, the results of this paper and in particular the uncertainty principle are fundamental and place restrictions on the types of intensity profiles that can be achieved through linear phase shaping alone.

For specific applications and in particular those requiring high power beams it may be necessary to consider the off-axis electric field and nonlinear interactions. Equation (3.14) gives an asymptotic result indicating that the intensity pattern near the target distance will form a Bessel-like function. Numerical

evidence indicates that for critical collapse of the beam to occur the power in the central core of the Bessel function must be near that of the Townes profile [51]. For the applications we considered, it follows from Equation (2.4) that the initial peak intensity of the ring beam E_0^2 is much smaller than the target peak intensity E_T^2 of the generated Bessel beam and hence Kerr nonlinearities will be negligible until the ring beam is focused into the Bessel-like pattern. Predicting the filamentation patterns of a beam after critical collapse is a challenging problem and perhaps the nonlinear geometrical optics method presented in [54] could be used in conjunction with our methods near the target distance. The full effect of the Kerr nonlinearities will be addressed in subsequent publications. Additionally, for propagation of the beam over ranges of 1 km it will be necessary to consider the effects of turbulence in the atmosphere which is beyond the scope of this paper.

Appendix A. Radially symmetric solutions to the paraxial wave equation

Consider the initial value problem with radially symmetric initial data:

$$\begin{cases} \frac{\partial E}{\partial z} = \frac{i}{2k} \Delta_{\perp} E \\ E(r, 0) = E_0 f(r) \end{cases}, \quad (\text{A.1})$$

where f is a smooth function with compact support. If we let $\mathcal{H}[g](k_{\perp})$ and $\mathcal{H}^{-1}[G](r)$ denote the Hankel transform and its inverse defined by

$$\mathcal{H}[g](k_{\perp}) = \int_0^{\infty} g(r) J_0(r k_{\perp}) dr \text{ and } \mathcal{H}^{-1}[G](r) = \int_0^{\infty} G(k_{\perp}) J_0(r k_{\perp}) k_{\perp} dk_{\perp} \quad (\text{A.2})$$

then the solution to the initial value problem is given by

$$E(r, z) = \int_0^{\infty} E_0 \mathcal{H}[f(r)](k_{\perp}) \exp\left(-\frac{i k_{\perp}^2 z}{2k}\right) J_0(r k_{\perp}) k_{\perp} dk_{\perp}. \quad (\text{A.3})$$

Noting that

$$\mathcal{H}^{-1}\left[\exp\left(-\frac{i k_{\perp}^2}{2k}\right)\right](r) = -\frac{ik}{z} \exp\left(\frac{ikr^2}{2z}\right) \quad (\text{A.4})$$

it follows from the convolution theorem for Hankel transforms [55] that

$$E(r, z) = -\frac{ik}{2\pi z} \int_0^{2\pi} \int_0^{\infty} f(\rho) e^{\frac{ik}{2z}(r^2 - 2r\rho(\cos(\theta)\cos(\phi) + \sin(\theta)\sin(\phi)) + \rho^2)} \rho d\rho d\phi. \quad (\text{A.5})$$

$$= -\frac{ik}{z} \int_0^{\infty} E_0 f(\rho) \exp(i\phi(\rho)) \exp\left(\frac{ik(r^2 + \rho^2)}{2z}\right) J_0\left(\frac{k\rho r}{z}\right) \rho d\rho. \quad (\text{A.6})$$

Acknowledgments: The authors acknowledge funding support under the MURI AFOSR grant FA9550-10-0561. C.D. acknowledges funding support from AFOSR under the grant FA9550-10-1-0394 and S.V. acknowledges support from the NSF grant 0807501. The authors wish to thank Ewan Wright for many useful discussions and bringing to our attention reference [22] and we would like to thank Colm Dineen who constructed Figure 2(b). The authors would also like to thank the two anonymous referees who reviewed this paper. Their comments greatly improved the organization and the presentation of our results.

References

References

- [1] T. Planchon, L. Gao, D. E. Milkie, M. W. Davidson, J. A. Galbraith, C. G. Galbraith, E. Betzig, Rapid three-dimensional isotropic imaging of living cells using Bessel beam plane illumination, *Nature Methods* 8 (2011) 417–423.
- [2] J. Arlt, V. Garcés-Chávez, W. Sibbett, K. Dholakia, Optical micromanipulation using a Bessel light beam, *Optics Communications* 197 (4-6) (2001) 239–245.
- [3] F. Courvoisier, J. Zhang, M. K. Bhuyan, M. Jacquot, J. M. Dudley, Applications of femtosecond Bessel beams to laser ablation, *Appl. Phys. A*.
- [4] M. Mills, M. Kolesik, D. Christodoulides, Dressed optical filaments, *Optics letters* 38 (1) (2013) 25–27.
- [5] P. Polynkin, M. Kolesik, A. Roberts, D. Faccio, P. Di Trapani, J. Moloney, Generation of extended plasma channels in air using femtosecond Bessel beams, *Opt Express* 16 (20) (2008) 15733–15740.
- [6] K. Stelmaszczyk, P. Rohwetter, G. Méjean, J. Yu, E. Salmon, J. Kasparian, R. Ackermann, J.-P. Wolf, L. Woste, Long-distance remote laser-induced breakdown spectroscopy using filamentation in air, *Applied Physics Letters* 85 (18) (2004) 3977–3979.
- [7] P. Rohwetter, K. Stelmaszczyk, L. Wöste, R. Ackermann, G. Méjean, E. Salmon, J. Kasparian, J. Yu, J.-P. Wolf, Filament-induced remote surface ablation for long range laser-induced breakdown spectroscopy operation, *Spectrochimica Acta Part B: Atomic Spectroscopy* 60 (7) (2005) 1025–1033.
- [8] L. Rayleigh, Xxix. on images formed without reflection or refraction, *The London, Edinburgh, and Dublin Philosophical Magazine and Journal of Science* 11 (67) (1881) 214–218.
- [9] A. C. Newell, J. V. Moloney, *Nonlinear optics*, Addison-Wesley Redwood City, 1992.

- [10] R. Grella, Fresnel propagation and diffraction and paraxial wave equation, *Journal of Optics* 13 (6) (1982) 367.
- [11] J. Durnin, Exact solutions for nondiffracting beams. i. the scalar theory, *J. Opt. Soc. Am. A* 4 (4) (1987) 651–654.
- [12] J. Durnin, J. Miceli Jr, J. Eberly, Diffraction-free beams, *Physical Review Letters* 58 (15) (1987) 1499–1501.
- [13] J. C. Gutiérrez-Vega, M. Iturbe-Castillo, S. Chávez-Cerda, Alternative formulation for invariant optical fields: Mathieu beams, *Optics letters* 25 (20) (2000) 1493–1495.
- [14] M. A. Bandres, J. C. Gutiérrez-Vega, S. Chávez-Cerda, Parabolic non-diffracting optical wave fields, *Optics letters* 29 (1) (2004) 44–46.
- [15] F. Gori, G. Guattari, C. Padovani, Bessel-Gauss beams, *Optics Communications* 64 (6) (1987) 491–495.
- [16] J. C. Gutiérrez-Vega, M. A. Bandres, et al., Helmholtz-gauss waves, *JOSA A* 22 (2) (2005) 289–298.
- [17] T. Graf, D. Christodoulides, M. S. Mills, J. Moloney, S. C. Venkataramani, E. M. Wright, Propagation of Gaussian-apodized paraxial beams through first-order optical systems via complexcoordinate transforms and ray transfer matrices, *J. Opt. Soc. Am. A* 29 (9) (2012) 1860–1869.
- [18] L. Niggel, T. Lanzl, M. Maier, Properties of bessel beams generated by periodic gratings of circular symmetry, *JOSA A* 14 (1) (1997) 27–33.
- [19] D. McGloin, K. Dholakia, Bessel beams: diffraction in a new light, *Contemporary Physics* 46 (1) (2005) 15–28.
- [20] Z. Bouchal, J. Wagner, M. Chlup, Self-reconstruction of a distorted non-diffracting beam, *Optics communications* 151 (4) (1998) 207–211.
- [21] T. Graf, J. Moloney, S. Venkataramani, Asymptotic analysis of weakly nonlinear bessel-gauß beams, *Physica D: Nonlinear Phenomena*.
- [22] V. Bagini, F. Frezza, M. Santarsiero, G. Schettini, G. S. Spagnolo, Generalized bessel-gauss beams, *Journal of Modern Optics* 43 (6) (1996) 1155–1166.
- [23] T. Čizmár, K. Dholakia, Tunable bessel light modes: engineering the axial propagation, *Optics express* 17 (18) (2009) 15558–15570.
- [24] D. C. Dobson, Phase reconstruction via nonlinear least-squares, *Inverse Problems* 8 (4) (1992) 541.
- [25] V. Kotlyar, P. Seraphimovich, V. Soifer, An iterative algorithm for designing diffractive optical elements with regularization, *Optics and lasers in engineering* 29 (4) (1998) 261–268.

- [26] O. Ripoll, V. Kettunen, H. P. Herzig, Review of iterative fourier-transform algorithms for beam shaping applications, *Optical Engineering* 43 (11) (2004) 2549–2556.
- [27] M. Pasienski, B. Demarco, A high-accuracy algorithm for designing arbitrary holographic atom traps, *Optics Express* 16 (3) (2008) 2176–2190.
- [28] R. A. Gonsalves, Phase retrieval and diversity in adaptive optics, *Optical Engineering* 21 (1982) 829–832.
- [29] C. D. J. Fienup, Phase retrieval and image reconstruction for astronomy, *Image Recovery: Theory and Application*, ed. by H. Stark, Academic Press, San Diego (1987) 231–275.
- [30] R. Trebino, D. J. Kane, Using phase retrieval to measure the intensity and phase of ultrashort pulses: frequency-resolved optical gating, *JOSA A* 10 (5) (1993) 1101–1111.
- [31] J. S. Liu, M. R. Taghizadeh, Iterative algorithm for the design of diffractive phase elements for laser beam shaping, *Opt Lett* 27 (16) (2002) 1463.
- [32] A. Rundquist, A. Efimov, D. H. Reitze, Pulse shaping with the Gerchberg-Saxton algorithm, *J. Opt. Soc. Am. B* 19 (10) (2002) 2468–2478.
- [33] R. W. Gerchberg, W. O. Saxton, Phase determination from image and diffraction plane pictures in the electron microscope, *Optik* 35 (1972) 237–246.
- [34] J. R. Fienup, Reconstruction of a complex-valued object from the modulus of its Fourier transform using a support constraint, *J. Opt. Soc. Am. A*.
- [35] D. R. Luke, J. V. Burke, R. G. Lyon, Optical wavefront reconstruction: Theory and numerical methods, *SIAM review* 44 (2) (2002) 169–224.
- [36] J. R. Fienup, Phase retrieval algorithms: a comparison, *Applied optics* 21 (15) (1982) 2758–2769.
- [37] D. Youla, Mathematical theory of image restoration by the method of convex projections, *Image Recovery: Theory and Application* (1987) 29–77.
- [38] H. H. Bauschke, P. L. Combettes, D. R. Luke, Phase retrieval, error reduction algorithm, and fienup variants: a view from convex optimization, *JOSA A* 19 (7) (2002) 1334–1345.
- [39] J. Fienup, C. Wackerman, Phase-retrieval stagnation problems and solutions, *JOSA A* 3 (11) (1986) 1897–1907.
- [40] C. Wackerman, A. Yagle, Use of fourier domain real-plane zeros to overcome a phase retrieval stagnation, *JOSA A* 8 (12) (1991) 1898–1904.

- [41] J. Rubinstein, G. Wolansky, A variational principle in optics, *JOSA A* 21 (11) (2004) 2164–2172.
- [42] L. Romero, F. Dickey, Lossless laser beam shaping, *JOSA A* 13 (4) (1996) 751–760.
- [43] A. T. Friberg, Stationary-phase analysis of generalized axicons, *JOSA A* 13 (4) (1996) 743–750.
- [44] L. A. Romero, F. M. Dickey, The mathematical and physical theory of lossless beam shaping, *Optical Engineering-New York-Marcel Dekker Incorporated-* 70 (2000) 21–118.
- [45] L. C. Evans, Weak convergence methods for nonlinear partial differential equations, American mathematical society Providence, 1990.
- [46] R. E. Paley, N. Wiener, Fourier transforms in the complex domain, Vol. 19, Oxford University Press, 1934.
- [47] G. B. Folland, A. Sitaram, The uncertainty principle: a mathematical survey, *Journal of Fourier Analysis and Applications* 3 (3) (1997) 207–238.
- [48] P. D. Miller, Applied asymptotic analysis, Vol. 75, American Mathematical Soc., 2006.
- [49] E. H. Lieb, M. Loss, Analysis, volume 14 of graduate studies in mathematics, American Mathematical Society, Providence, RI, 4.
- [50] J. W. Goodman, Introduction to Fourier optics, Roberts and Company Publishers, 2005.
- [51] G. Fibich, A. L. Gaeta, Critical power for self-focusing in bulk media and in hollow waveguides, *Optics letters* 25 (5) (2000) 335–337.
- [52] P. J. Wrzesinski, D. Pestov, V. V. Lozovoy, J. R. Gord, M. Dantus, S. Roy, et al., Group-velocity-dispersion measurements of atmospheric and combustion-related gases using an ultrabroadband-laser source, *Opt. Express* 19 (6) (2011) 5163–5171.
- [53] C. G. Durfee, J. Gemmer, J. V. Moloney, Phase-only shaping algorithm for gaussian-apodized besel beams, *Optics Express* 21 (13) (2013) 15777–15786.
- [54] N. Gavish, G. Fibich, L. T. Vuong, A. L. Gaeta, Predicting the filamentation of high-power beams and pulses without numerical integration: a non-linear geometrical optics method, *Physical Review A* 78 (4) (2008) 043807.
- [55] A. D. Poularikas, Transforms and applications handbook, CRC press, 2009.